Article

Cell Reports

Burst-Dependent Bidirectional Plasticity in the Cerebellum Is Driven by Presynaptic NMDA Receptors

Graphical Abstract

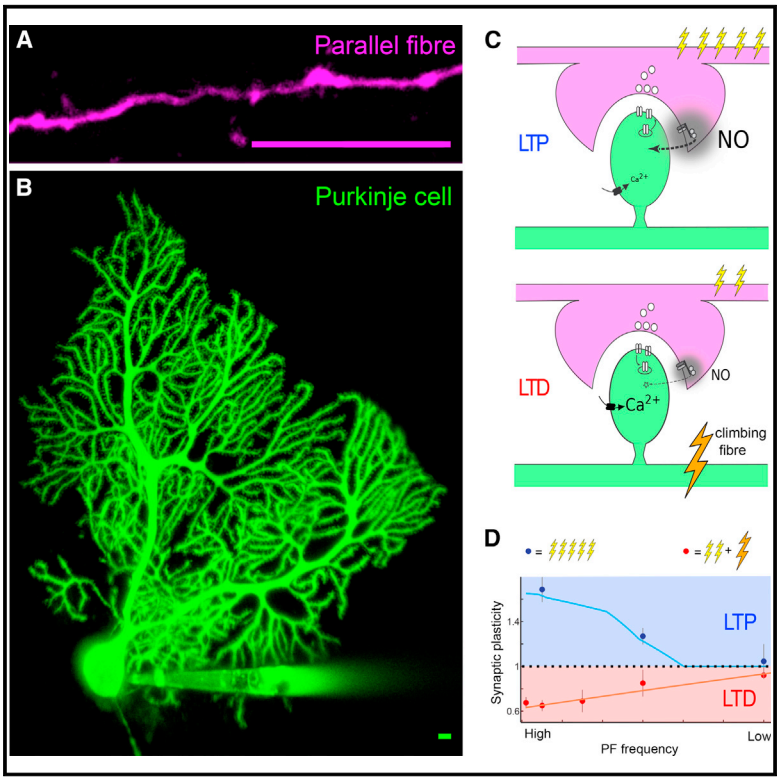

Highlights

- The input firing patterns determine cerebellar bidirectional synaptic plasticity
- There is an obligatory involvement of presynaptic NMDA receptors in parallel fibers
- NMDA receptor activation is pattern-dependent
- A constrained and predictive model encompasses a unified "synaptic plasticity rule"

Authors

Guy Bouvier, David Higgins, Maria Spolidoro, ..., Boris Barbour, Nicolas Brunel, Mariano Casado

Correspondence

casado@biologie.ens.fr

In Brief

Bouvier et al. show that presynaptic NMDA receptor activation at the cerebellar synapse between parallel fibers and Purkinje cells is linked to the bidirectional plasticity rule. Combined electrophysiology, calcium imaging, and mathematical modeling generate a comprehensive view of the link between signaling mechanisms and the definition of the synaptic plasticity rule.

Bouvier et al., 2016, Cell Reports *15*, 104–116
April 5, 2016
http://dx.doi.org/10.1016/j.celrep.2016.03.004

CellPress

OPEN ACCESS
CellPress

Cell Reports
Article

Burst-Dependent Bidirectional Plasticity in the Cerebellum Is Driven by Presynaptic NMDA Receptors

Guy Bouvier,[1] David Higgins,[1,2,3] Maria Spolidoro,[1,4] Damien Carrel,[1,5] Benjamin Mathieu,[1] Clément Léna,[1] Stéphane Dieudonné,[1] Boris Barbour,[1] Nicolas Brunel,[2] and Mariano Casado[1,*]

[1]Ecole Normale Supérieure, Institut de Biologie de l'ENS (IBENS), Inserm U1024, CNRS UMR 8197, Paris 75005, France
[2]Departments of Statistics and Neurobiology, University of Chicago, Chicago, IL 60637, USA
[3]Present address: Modelling of Cognitive Processes, Berlin Institute of Technology and Bernstein Center for Computational Neuroscience, 10115 Berlin, Germany
[4]Present address: Friedrich Miescher Institute for Biomedical Research, 4058 Basel, Switzerland
[5]Present address: Neurophotonics Laboratory, CNRS UMR8250, Université Paris Descartes, 75270 Paris, France
*Correspondence: casado@biologie.ens.fr
http://dx.doi.org/10.1016/j.celrep.2016.03.004

SUMMARY

Numerous studies have shown that cerebellar function is related to the plasticity at the synapses between parallel fibers and Purkinje cells. How specific input patterns determine plasticity outcomes, as well as the biophysics underlying plasticity of these synapses, remain unclear. Here, we characterize the patterns of activity that lead to postsynaptically expressed LTP using both in vivo and in vitro experiments. Similar to the requirements of LTD, we find that high-frequency bursts are necessary to trigger LTP and that this burst-dependent plasticity depends on presynaptic NMDA receptors and nitric oxide (NO) signaling. We provide direct evidence for calcium entry through presynaptic NMDA receptors in a subpopulation of parallel fiber varicosities. Finally, we develop and experimentally verify a mechanistic plasticity model based on NO and calcium signaling. The model reproduces plasticity outcomes from data and predicts the effect of arbitrary patterns of synaptic inputs on Purkinje cells, thereby providing a unified description of plasticity.

INTRODUCTION

Synaptic plasticity is thought to be the cellular mechanism underlying learning and memory and has been the subject of intense experimental and theoretical research. The experimental work has led to detailed knowledge of the receptors and signaling pathways involved in the induction of different types of synaptic plasticity (Squire and Kandel, 2009). In parallel, theoretical studies have built "plasticity rules", formal descriptions linking spike timings to changes in synaptic efficacy, such as the spike-timing-dependent plasticity (STDP) rule (Gerstner et al., 1996). However, these plasticity rules are generally quite abstract, and their link to underlying biophysical mechanisms is often unclear. The best known synaptic plasticity mechanisms are linked to N-methyl-D-aspartate receptor (NMDAR) function. NMDARs are biophysical coincidence detectors of glutamate and membrane depolarization (Nowak et al., 1984). The activation of postsynaptic NMDARs defines learning rules where the relative timing of pre- and postsynaptic activity is a key parameter (Debanne et al., 1994; Sjöström et al., 2003; Fino et al., 2010). In the few cases where the participation of presynaptic NMDARs has been proposed, these have invariably been involved in presynaptically expressed LTD (Sjöström et al., 2003; Rodríguez-Moreno and Paulsen, 2008).

Cerebellar parallel fiber to Purkinje cell (PF-PC) synaptic plasticity follows non-Hebbian plasticity rules (Jörntell and Hansel, 2006). We have previously reported that the induction of postsynaptically expressed PF-PC LTD requires PF bursting activity (at least pairs of spikes) (Bidoret et al., 2009) and is linked to the presumed presence of presynaptic NMDARs (Casado et al., 2002). Here, we characterize the activity requirements for postsynaptic LTP induction, investigate the signaling pathways involved, and examine in detail the potential involvement of NMDARs. Surprisingly, we found that LTP induction shares many properties with LTD induction, including a similar frequency-dependence on presynaptic activity and an absolute requirement for NMDAR activation and nitric oxide (NO) production. In contrast with other synapses (Fujino and Oertel, 2003; Bender et al., 2006; Fino et al., 2010), our data indicate that LTP and LTD share signaling mechanisms. These involve presynaptically produced NO and postsynaptic Ca rises. Supporting the notion that the frequency dependence of plasticity arises from the involvement of presynaptic NMDARs, we provide direct evidence for Ca influx through presynaptic NMDARs in PFs, clarifying a long-lasting controversy (Casado et al., 2002; Shin and Linden, 2005; Bidoret et al., 2009; Wang et al., 2014).

Based on our data and relevant data from the literature, we propose a mechanistic plasticity rule. This deliberately parsimonious rule can be used to interpret and predict the plasticity arising from arbitrary patterns of PF and climbing fiber (CF) activity. Our results support the notion that bidirectional synaptic plasticity depends on multi-spike activity patterns in an intricate fashion (Sjöström et al., 2001; Froemke and Dan, 2002).

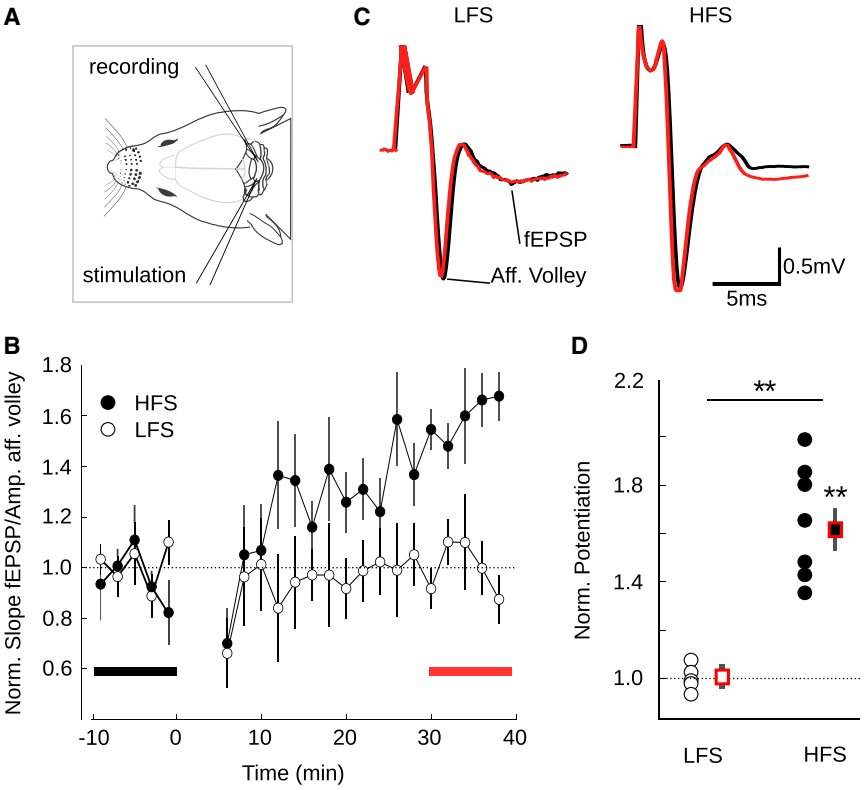

Figure 1. High-Frequency Parallel Fiber Activity Is Required for LTP Induction In Vivo

(A) Diagram of the experimental preparation. A cranial window was opened above the cerebellum of anaesthetized rats. The PFs were stimulated with a tungsten microelectrode. The field EPSPs were recorded with a second microelectrode.

(B) Time course of the normalized ratios (slope of the field EPSP/amplitude of the afferent volley). The HFS plasticity induction: 15 pulses at 100 Hz repeated at 1 Hz for 5 min (black, n = 7). The LFS plasticity induction: 15 pulses at 16.7 Hz repeated at 1 Hz for 5 min (white, n = 5). The bottom bars indicate when the baseline (black) and after plasticity induction (red) traces were averaged to calculate plasticity. The ratios were first normalized and then averaged. The data represent mean ± SEM.

(C) Representative recordings from the experiments in (B) and (D). The traces are averages of 15 sweeps before (black) and after (red) LFS or HFS plasticity induction.

(D) Summary of normalized ratios after LFS (white) or HFS (black) induction. The squares are mean ± SEM. A ratio of 1 indicates no change.

RESULTS

Precise Temporal Structure of PF Stimulation Is Essential for LTP Induction

Cerebellar granule cells fire in vivo at a wide range of frequencies that can reach 1 kHz (Chadderton et al., 2004). Repetitive high-frequency PF stimulation has been shown to induce LTP at PF-PC synapses both in vivo (Wang et al., 2009) and in vitro (Lev-Ram et al., 2002; Coesmans et al., 2004; Ly et al., 2013). In order to characterize the frequency dependence of LTP induction, we first evaluated the impact of PF frequency on plasticity induction at PF-PC synapses in vivo by recording local field potentials in anesthetized rats (Figure 1A). High-frequency stimulation (HFS, 15 pulses at 100 Hz repeated at 1 Hz for 5 min) resulted in robust LTP (Figures 1B–1D; 157 ± 9%, n = 7, and p = 0.001). In contrast, low-frequency stimulation (LFS, 15 pulses at 16.7 Hz repeated at 1 Hz for 5 min) resulted in no LTP (99 ± 5%, n = 5, p = 0.66, and p = 0.0025 versus control). As in Wang et al. (2009), long-term plasticity in vivo develops gradually. Thus, LTP induced at PF-PC synapses in vivo is dependent on the firing frequency of the presynaptic element.

In order to dissect the mechanisms of this frequency dependence, we quantified the impact of different PF activity patterns on LTP induction in vitro. We examined in acute cerebellar slices the influence of varying the intraburst frequency and the number of stimuli in a burst. The plasticity protocols consisted of 300 repeats at 1 Hz of bursts of a small number of stimuli (Figures 2A and 2B). A marked increase of the excitatory postsynaptic current (EPSC) charge was observed immediately upon cessation of the induction protocol (Figure 2C). Following this short-term change, the charge stabilized at different levels after 30 min, the time point at which we measured the degree of long-term plasticity. The short-term change was associated with a transient decrease of paired-pulse facilitation (PPF; Figure 2D; 86 ± 2% of the control PPF value 5 min after induction, but 102 ± 2% 30 min later). Changes in PPF have been shown to be associated with presynaptic phenomena (Manabe et al., 1993). The transient decrease in PPF observed here is thus reminiscent of the presynaptic short-term potentiation described by Goto et al. (2006). Short-term changes differ in vivo and in vitro. This may be due to the presence of intact inhibition in vivo while in vitro inhibition is blocked by bicuculline. The magnitude of long-term changes was found to depend on the intraburst frequency over a range of physiologically relevant PF frequencies (Chadderton et al., 2004) (Figures 2C, 2E, and 2F). 200 Hz bursts of five pulses induced a robust LTP (Figures 2C, 2E, and 2F; 169 ± 11%, n = 18, and p = 4.7 × 10^{-8}), which persisted for at least 1 hr (168 ± 7%, n = 5, and p = 0.0075). LTP could be induced with different postsynaptic Ca buffering capacities (163 ± 8%, n = 5 with 0.1 mM EGTA, versus 169 ± 11%, with 5 mM 1,2-Bis(2-aminophenoxy) ethane-N,N,N′,N′-tetraacetic acid (BAPTA), n = 18, and p = 0.64; data not shown). Protocols using 33.3 Hz bursts induced a smaller LTP than those using 200 Hz bursts (127 ± 7%, n = 6, p = 0.0028, and p = 0.012 versus 200 Hz). 16.7 Hz bursts were ineffective for LTP induction (104 ± 15%, n = 6, p = 0.35, and p = 0.0058 versus 200 Hz). Thus, LTP amplitude is dependent on the spike frequency during burst stimulation of PFs (ANOVA p = 0.0084 for 200 Hz–33.3 Hz–16.7 Hz comparison). In all conditions the PPF was unaffected 30 min after the induction protocol (Figure 2D; 96 ± 3% and 103 ± 2% of the control

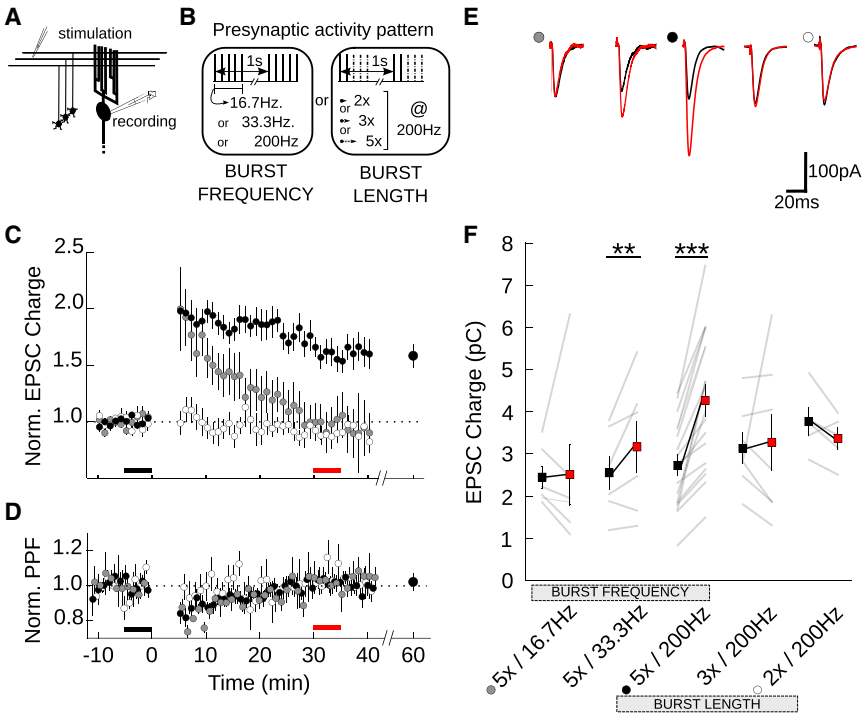

Figure 2. Bursts of High-Frequency PF Activity Are Required for LTP Induction

(A) Diagram of the experimental preparation. The PFs were stimulated in the molecular layer. The PCs were recorded in the whole-cell configuration.

(B) Plasticity was induced with repetitive PF stimulation (bursts of 2, 3, or 5 pulses, repeated 300 times at 1 Hz). Several intraburst frequencies were tested (16.7, 33.3, or 200 Hz).

(C) Time course of the normalized EPSC charge in experiments where plasticity was induced with 5-pulse bursts and intraburst frequencies of 200 Hz (black) or 16.7 Hz (gray) or 2-pulse bursts of intraburst frequency 200 Hz (open symbols). For the 5×/200 Hz experiment, LTP was also recorded at longer times (n = 5, large black dot).

(D) Time course of the normalized PPF for experiments in (C).

(E) Representative EPSCs. The traces are averages of 15 sweeps immediately before (black) and 30 min after (red) LTP induction. The dots beside the traces are the same as in (C).

(F) EPSC charge before and after plasticity induction for all individual experiments (same order and color code as in E). The plasticity induction consisted of stimulation with five pulses at 16.7 Hz (n = 6), five pulses at 33.3 Hz (n = 6), five pulses at 200 Hz (n = 18), three pulses at 200 Hz (n = 7), or two pulses at 200 Hz (n = 5). The squares are mean ± SEM in picocoulombs.

value, for 33.3 Hz and 16.7 Hz, respectively). The absence of PPF changes after LTP induction is consistent with a postsynaptic site of expression (Manabe et al., 1993; Lev-Ram et al., 2002; Coesmans et al., 2004).

We then varied the number of stimuli in 200 Hz bursts (Figure 2B). Five pulses induced robust LTP, whereas two pulses did not (two pulses, 94 ± 5%, n = 5, and p = 0.39 and p = 0.0058 for two versus five pulses; Figures 2C, 2E, and 2F). A 3-pulse protocol was also ineffective in inducing LTP (104 ± 19%, n = 7, p = 0.68, and p = 0.002 versus five pulses; Figures 2E and 2F). Thus, synapses that receive high-frequency bursts with five pulses are selectively potentiated compared to those receiving bursts with three or fewer pulses.

Long-Term Potentiation Depends on NMDARs and Nitric Oxide

We next sought to identify the molecular constraints defining the plasticity rule characterized above. Burst stimulation of PFs in the molecular layer has been found to activate metabotropic glutamate receptors (mGluR1). Since mGluR1 activation has been reported to play a role in PF-PC LTD induction (Wang et al., 2000), we decided to check for a putative role of mGluR1 activation in LTP induction. We performed a set of experiments in the presence of the non-competitive antagonist CPCCOEt (50 μM). LTP could still be induced in these conditions (Figure S1; 196 ± 25%, n = 5, p = 0.0075, and p = 0.29 versus control LTP). This result is in line with previous studies (Namiki et al., 2005).

Activation of a compact beam of PFs following molecular layer stimulation may increase glutamate spillover in a non-physiological manner (Marcaggi and Attwell, 2007). We therefore tested the ability of granule cell layer (GCL) stimulation, which elicits a sparse input to the PC, to induce LTP. We found that a similar degree of LTP was induced (Figure S1; 213 ± 31%, n = 5, p = 0.0075, and p = 0.20 versus molecular layer stimulation). It is thus unlikely that glutamate spillover or any other form of crosstalk between synapses plays a major role during LTP induction.

NMDAR-dependent NO production could be considered a plausible candidate mechanism since high-frequency PF activity is required for LTP (Figures 1 and 2), HFS has been proposed to activate NMDARs in PFs (Bidoret et al., 2009), and PF bursting activity produces NO in a NMDAR-dependent manner (Wang et al., 2014). We thus checked the involvement of NMDARs in LTP induction. 100 μM D-APV, a NMDAR antagonist, fully blocked LTP (Figures 3A, 3C, and 3D; 102 ± 8%, n = 7, p = 0.17, and p = 1.66 × 10^{-5} versus control LTP) without affecting short-term potentiation. As in control experiments, this short-term potentiation was associated with a transient decrease in PPF (Figure 3B; 80 ± 4% of control after 5 min, 100 ± 4% 30 min later). NMDAR activation is involved in the induction rather than expression of LTP, since APV still prevents plasticity when its application is restricted to the baseline and induction periods and washed out after plasticity induction (102 ± 11%, n = 5, p = 0.31, and p = 0.003 versus control LTP). Thus, LTP induction is NMDAR dependent.

Calcium entry through NMDARs requires two simultaneous conditions: activation by glutamate binding and depolarization to relieve the Mg block of the channel (Nowak et al., 1984). The time window for this coincidence depends critically on the kinetic properties of NMDARs, which in turn depend on their subunit composition (Bidoret et al., 2009). To determine the

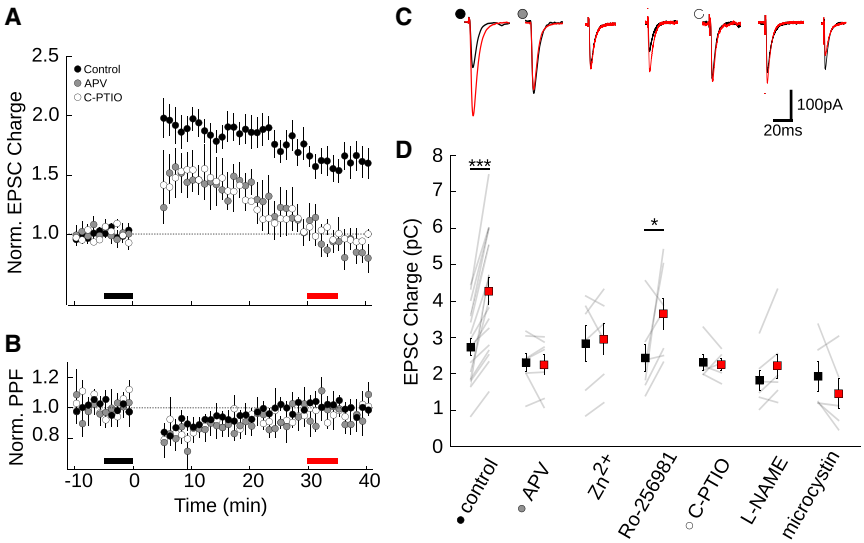

Figure 3. LTP Depends on GluN2A Containing NMDARs and Nitric Oxide

(A) Time course of the normalized EPSC charge in control conditions (black) or in the presence of CPTIO (open) or D-APV (gray).

(B) Time course of the normalized PPF for experiments in (A).

(C) Representative recordings before (black) and after (red) LTP induction in the different conditions shown in (D).

(D) EPSC charge before and after plasticity induction for all individual experiments in control conditions (five pulses at 200 Hz, repeated 300 times at 1 Hz, and n = 18, same as Figure 2) or in the presence of 100 μM D-APV (n = 7), 300 nM Zn^{2+} (n = 6), 300 nM Ro25-6981 (n = 6), 100 μM CPTIO (n = 5), 100 μM L-NAME (n = 6) in the bath, or 5 μM microcystin LR in the patch pipette (same order and color code as in C). The squares are mean ± SEM.

subunit composition of the NMDARs contributing to LTP induction, we used subunit-specific non-competitive antagonists. Buffered nanomolar Zn^{2+} specifically inhibits GluN2A-containing NMDARs (Paoletti et al., 1997). In the presence of 300 nM free Zn^{2+}, the 5-pulse protocol failed to induce LTP (Figures 3C and 3D; 120 ± 10%, n = 6, p = 0.35, and p = 0.012 versus control). In contrast, in the presence of the GluN2B-specific antagonist Ro25-6981, the same protocol still induced LTP (Figures 3C and 3D; 172 ± 27%, n = 6, p = 0.02, and p = 0.84 versus control). Therefore, GluN2A-, but not GluN2B, -containing NMDARs are required for LTP induction. The deactivation kinetics of GluN2A-containing NMDARs are much faster than those of GluN2B-bearing receptors and are consistent with the requirement for high-frequency bursts to induce LTP (Figures 1 and 2), similar to the NMDAR-dependency of LTD (Bidoret et al., 2009).

Postsynaptically expressed LTP has been shown to depend on NO signaling (Lev-Ram et al., 2002; Namiki et al., 2005). We verified the involvement of this signaling pathway in our experimental conditions (Figures 3A, 3C, and 3D). The presence of the NO scavenger c-PTIO (100 μM) fully prevented LTP (102 ± 7% and p = 0.00024 versus control LTP, p = 0.66 versus baseline, n = 5). The NOS inhibitor L-NAME (100 μM) strongly reduced LTP (121 ± 8% and p = 0.012 versus control LTP, p = 0.014 versus baseline, n = 6). Since PCs do not express NOS, whereas granule cells do (Bredt et al., 1990), the most plausible source of the NO required for the induction of LTP is the NOS expressed in PFs (we provide additional support for this conclusion below). Because the enzyme is Ca dependent and is often coupled to NMDARs (Christopherson et al., 1999), we further hypothesize that Ca entry through presynaptic NMDARs activates NO production from NOS in PFs, the NO then diffusing to the postsynaptic compartment, the PC spine.

Postsynaptic expression of LTP has also been shown to depend on PC phosphatase activity (Belmeguenai and Hansel, 2005). To verify the match between the LTP shown here and these previous reports, we checked the sensitivity of LTP induction to the presence of a phosphatase blocker, microcystin LR (Figures 3C and 3D). In the presence of 5 μM of this compound in the patch pipette, no LTP could be observed (77 ± 15% and p = 0.0009 versus control LTP, p = 0.11 versus baseline, n = 5).

The sensitivity of LTP induction to NMDAR antagonists is in contrast with previous reports (Wang et al., 2014; Piochon et al., 2010; Canepari and Vogt, 2008). To resolve this contradiction, we propose that slice orientation (sagittal or transverse) may have an important impact on the NMDAR-dependence of plasticity induction. Local electroporation of the tissue by the stimulation electrode (Hamann and Attwell, 1996; and imaging data below) has been shown to compromise presynaptic Ca dynamics and could bypass the need for presynaptic NMDAR activation to trigger NO production. This may correspond to the situation found in the sagittal slices used in previous studies, where the stimulation electrode was close to the recorded synapses. We performed a set of LTP experiments in sagittal slices to compare them with the equivalent experiments in transverse slices shown in Figures 2 and 3. LTP was induced in sagittal slices with the same protocol and solutions used in transverse slices (Figure S1). The amplitude of potentiation was similar (145 ± 8%, n = 12 in sagittal versus 169 ± 11%, n = 18 in transverse slices). However, LTP in sagittal slices was insensitive to NMDAR block (156 ± 13%, n = 8 in the presence of APV; Figure S1), in sharp contrast with the APV sensitivity of LTP induction in transverse slices (Figure 3). This result confirms the reported data in the literature (Wang et al., 2014; Piochon et al., 2010; Canepari and Vogt, 2008), but indicates that slice orientation may have a key impact on presynaptic Ca dynamics and the conditions of NO signaling to the recorded synapses.

It has been proposed that NMDARs located in other cerebellar cell types may be responsible for the NMDAR dependence of PF-PC plasticity induction. This includes NMDARs in molecular layer interneurons (Shin and Linden, 2005; Wang et al., 2014) and postsynaptic NMDARs at the CF-PC synapse (Piochon et al., 2010). To ascertain the location of the NMDARs involved in LTP induction, we produced mice lacking NMDARs specifically in granule cells. We crossed *BACα6Cre* mice with

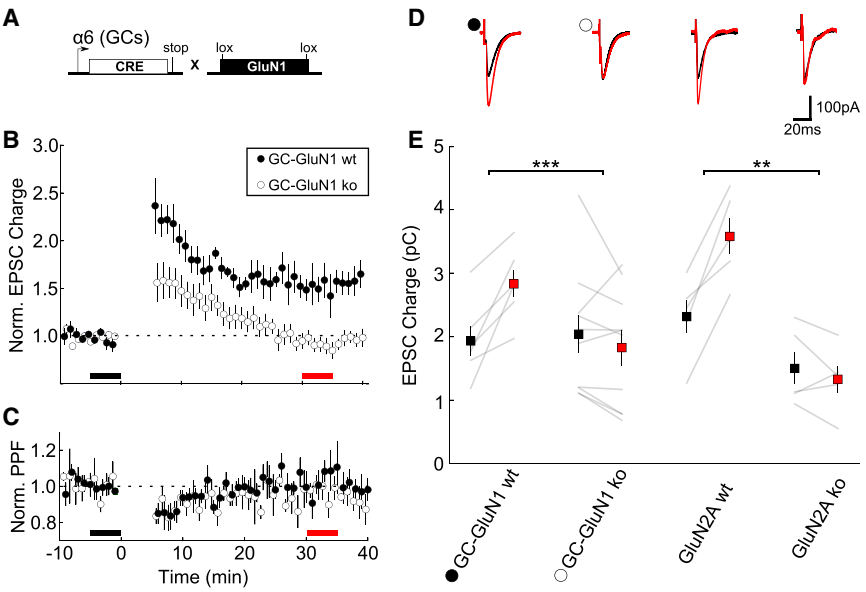

Figure 4. LTP Depends on NMDARs Located in PFs

(A) Schematic representation of the strategy to knock out the *GluN1* gene in cerebellar granule cells.

(B) Time course of the normalized EPSC charge in GC-GluN1wt (black) and GC-GluN1ko (open).

(C) Time course of the normalized PPF for experiments in (B).

(D) Representative recordings before (black) and after (red) LTP induction in the different conditions shown in (E). The dots beside the traces are the same as in (B).

(E) EPSC charge before and after plasticity induction for all individual experiments in GC-GluN1wt (n = 6), GC-GluN1ko (n = 10), GluN2Awt (n = 5), and GluN2Ako (n = 5) (same order and color code as in D). The squares are mean ± SEM.

GluN1 floxed mice (Figure 4A; Supplemental Information). Mice homozygous for the deleted *GluN1* allele were viable and their cerebellum appears to develop normally. LTP was abolished in these animals (91 ± 7%, n = 10 versus 163 ± 21%, n = 6 in slices from control animals *GluN1*$^{flox/flox}$ without Cre; Figures 4B–4E). This result shows that the NMDARs necessary for LTP induction at PF-PC synapses are located in the presynaptic granule cell and not at an alternative location.

To confirm the involvement of NMDARs containing GluN2A subunits in PF-PC LTP, we compared experiments performed on GluN2A KO mice to those performed on wild-type littermates. PF-PC synapses from wild-type mice expressed LTP in control conditions (165 ± 15%, n = 5, and p = 0.0075; Figures 4D and 4E) of the same amplitude as that from rats in control conditions (169 ± 11%, n = 18 from Figures 2C–2F; p = 0.1). In contrast, LTP was absent in slices from GluN2A KO mice (Figures 4D and 4E; 98 ± 13%, n = 5, and p = 0.66; wild-type versus KO, p = 0.01).

Presynaptic NMDARs Are Activated by LTP-Inducing Spike Patterns

We have previously reported that NMDAR subunits can be detected in presynaptic PFs by immunochemical techniques at both light and electron microscopy levels (Bidoret et al., 2009). However, direct evidence for NMDAR mediated Ca signaling in PFs was still lacking. In the absence of direct proof of functional presynaptic NMDARs in PFs, alternative hypotheses have been formulated to account for the dependence on NMDARs of LTD induction (Shin and Linden, 2005; Wang et al., 2014).

In order to monitor presynaptic Ca signals directly and to seek evidence of the activation of presynaptic NMDARs, we performed granule cell acute transgenesis through in vivo electroporation of a genetically encoded Ca indicator (GCaMP5G) and a morphological marker (mOrange). Fluorescence was measured using a 2-photon imaging system based on acousto-optic deflectors. Sparse subpopulations of granule cells expressed both fluorescent proteins throughout their somatodendritic compartments, ascending axons and PFs (Figure 5A). Extracellular stimulation in the vicinity of a fiber resulted in fluorescence transients in morphologically identified PF varicosities, reporting Ca entry (Figures 5B, 5C, S2A, and S2B). Beyond a certain distance from the stimulation electrode, these transients reported Ca dynamics during the action potential and were abolished by TTX or Cd^{2+}. However, in the vicinity of the stimulation electrode, the Ca signal was often larger, longer, and insensitive to channel blockers, which probably resulted from local electroporation (Figure S2D) (Hamann and Attwell, 1996). Thus, as for the electrophysiology recordings, we performed Ca imaging in transverse slices at a distance from the stimulation point sufficient to avoid spurious disturbance of the presynaptic Ca dynamics upon molecular layer stimulation. Bursts of 20–25 stimuli did not saturate the probe (Figures S2A and S2B). We measured Ca transients induced by 200 or 16.7 Hz bursts (Figures 5B and 5C). Calcium transients could be readily detected after stimulation at different frequencies. The size of the transient depended on the frequency (Figures 5B and 5C) and the length of the stimulation (Figures S2A and S2B), higher frequencies and longer trains resulting in larger Ca transients. Bath-applied APV produced no detectable effect on basal Ca levels (Figure S2C). However, APV reversibly decreased the average Ca transient when PFs were stimulated with 200 Hz bursts (HFS, 95 ± 1% APV versus baseline, n = 87 and p = 0.03), but not when PFs were stimulated with 16.7 Hz bursts (LFS, 101 ± 1%, n = 52 varicosities; APV versus baseline, p = 0.48; and APV HFS versus APV LFS, p = 0.04; Figure 5D). To ascertain the subunit-specific pharmacology of the receptors, we repeated the 200 Hz stimulation experiment in the continuous presence of 300 nM Zn. At this concentration, Zn is a specific inhibitor of GluN2A-containing NMDARs (Paoletti et al., 1997). Zn prevented the APV effect on Ca transients (95 ± 1% in control versus 103 ± 1% in Zn, n = 65 and p = 0.001).

Inspection of Ca responses of individual varicosities (Figure 5B) suggested that only some exhibited an APV-sensitive component. To examine this more quantitatively, we analyzed the distributions of the APV effect on presynaptic Ca responses

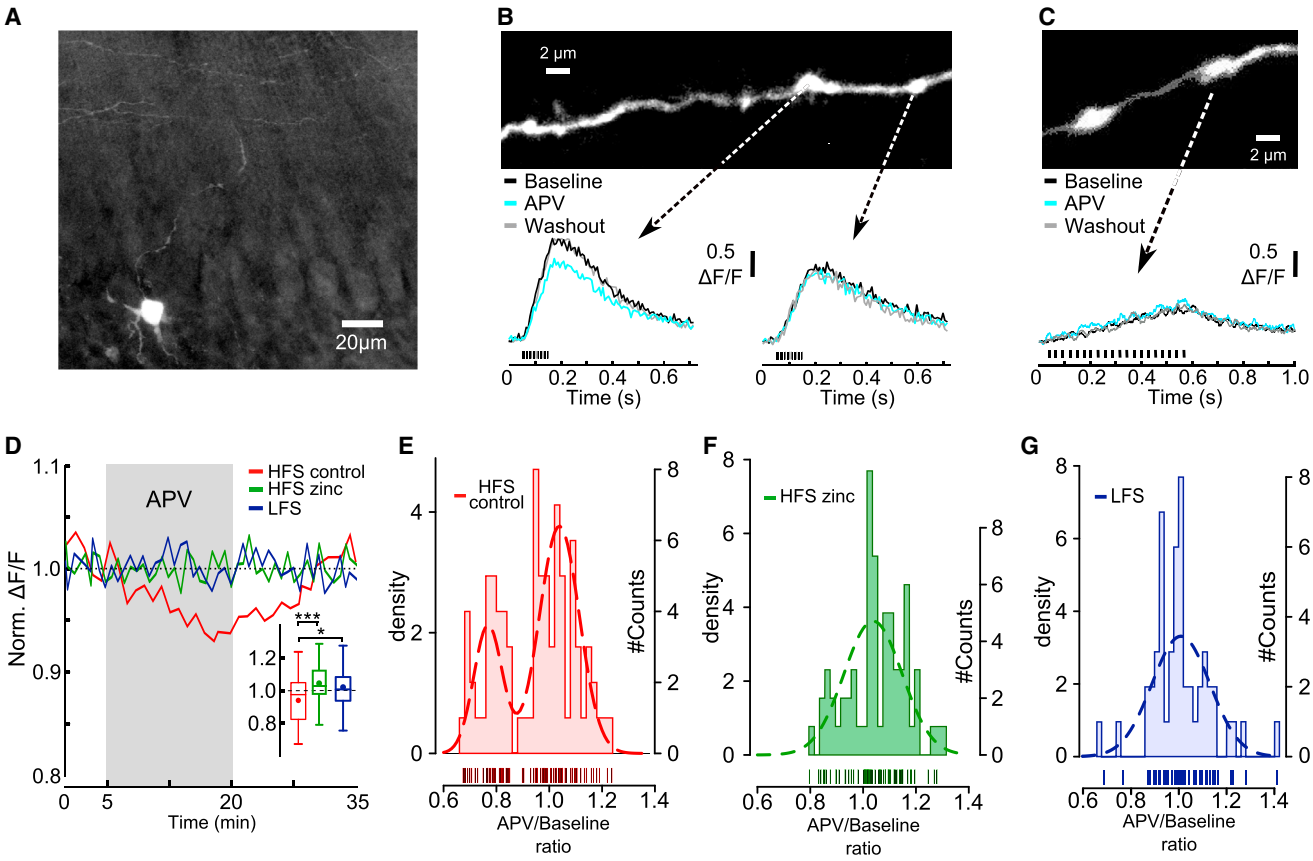

Figure 5. Calcium Imaging in Parallel Fibers

High-frequency bursts activate presynaptic NMDARs.

(A) Confocal stack projection (50 μm) showing granule cell somatodendritic compartments, ascending axons, and PFs in a transverse slice of a cerebellum electroporated with mOrange.

(B) 2-photon Ca imaging of GCAMP5G electroporated granule cells (top). A z-projection (30 planes, 0.4 μm step) of a PF expressing mOrange is shown. Representative fluorescence recordings after PF electrical stimulation are shown (bottom). The traces are averages of 15 sweeps before (black), during (cyan), and after (gray) bath application of 150 μM D-APV. The PF stimulation consisted of 20 pulses at 200 Hz every 15 s (HFS).

(C) Stimulation consisted of 20 pulses at 16.7 Hz every 15 s (LFS).

(D) Time course of the normalized ΔF/F in experiments with 200 Hz bursts in control conditions (HFS control in red, n = 87 varicosities), 200 Hz in the continuous presence of 300 nM Zn^{2+} (HFS zinc in green, n = 65 varicosities), or 16.7 Hz (LFS in blue, n = 52 varicosities). D-APV (150 μM) was bath applied between the 5th and 20th min. The box plot comparing the normalized effect of NMDAR block during HFS control (red), HFS in the presence of Zn (green), or LFS (blue) is shown in the inset. The mean (dot) and median (line) are shown.

(E) Only a fraction of PF varicosities are sensitive to NMDAR block by APV when stimulated at 200 Hz. Top: histogram of APV/baseline ΔF/F ratios (solid line) and estimated density of a finite mixture model (dashed line). Bottom: distribution of the total population.

(F) In the presence of 300nM Zn^{2+}, the Ca signal in PF varicosities is not sensitive to NMDAR block when stimulated at 200 Hz. Top: histogram of APV/baseline ΔF/F ratios (solid line) and estimated density of a finite mixture model (dashed line).

(G) The Ca signal in PF varicosities is not sensitive to NMDAR block during low-frequency stimulation (LFS). Top: histogram of APV/baseline ΔF/F ratios (solid blue line) and estimated density of the finite mixture model (dashed blue line).

to trains of stimuli (Figures 5E–5G) using finite mixture modeling, evaluated with both the Akaike information criterion and Bayes information criterion. This indicated the presence of a subgroup of reduced responses in APV at 200 Hz ($\mu1$ = 1.038, $\mu2$ = 0.768, σ = 0.075, and 0.054 and proportion = 0.713 and 0.287). The same analysis confirmed the absence of an APV effect on Ca signals at 16.7 Hz (only one Gaussian population; μ = 1.01 and σ = 0.12). We also found no support for the existence of more than one Gaussian component in the effect of APV for HFS in the presence of Zn (μ = 1.04 and σ = 0.11). No correlation was observed between the APV effect and basal fluorescence or ΔF/F in a varicosity (data not shown). Varicosities displaying APV-sensitivity at 200 Hz appeared to be randomly distributed even along the same fiber, as in the example shown in Figure 5B. Thus, high-frequency PF activity appears to induce NMDAR mediated Ca signals in a subset of PF varicosities. The receptors activated display a GluN2A-containing pharmacology.

A Unified Mechanistic Model of Plasticity at the PF-PC Synapse

Our results, combined with those in the literature, suggest that presynaptic NO production and postsynaptic Ca rises are

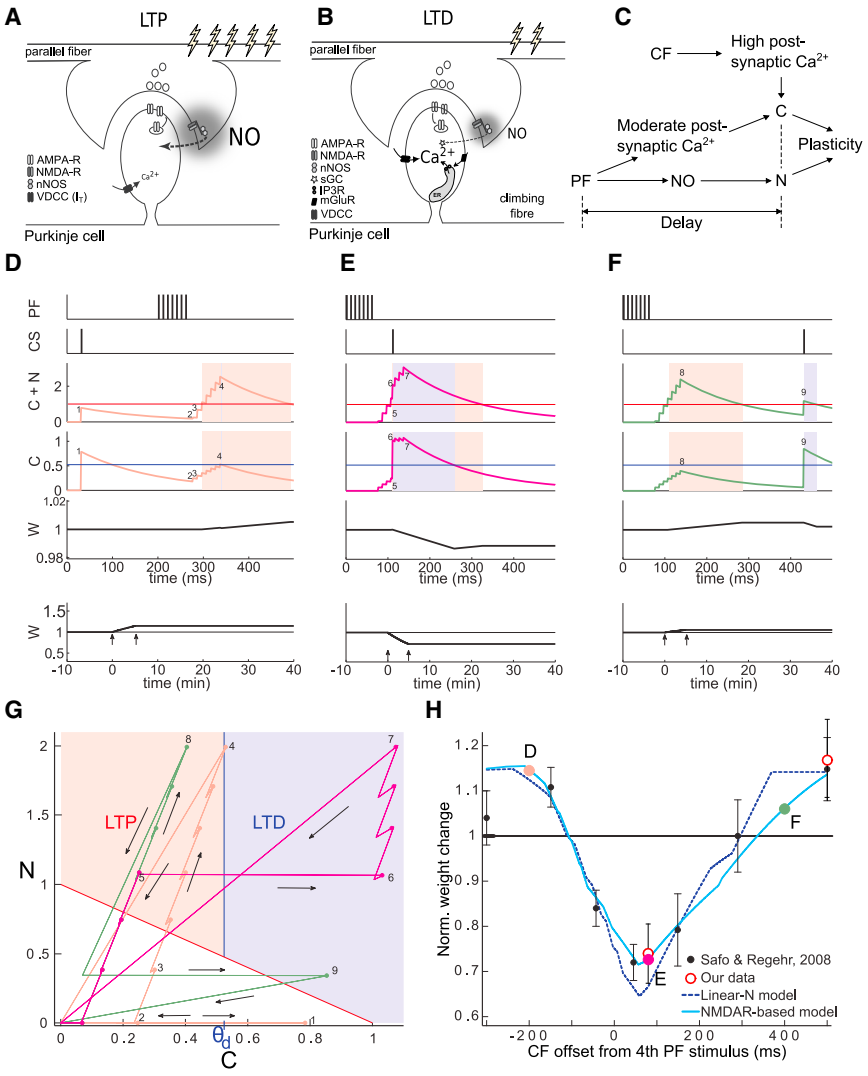

Figure 6. A Unified Model of PF-PC Bidirectional Synaptic Plasticity

(A) Diagram of LTP induction. A burst of five PF action potentials causes a moderate postsynaptic Ca rise and triggers release of NO from the presynaptic varicosity.

(B) Diagram of LTD induction. There are two PF action potentials that trigger postsynaptic Ca and NO signals, near conjunction with the CF, which produces a large postsynaptic Ca rise, induces LTD.

(C) The model is based on two plasticity variables, C and N, driven by postsynaptic Ca and NO. The CF activity results in large increases in postsynaptic C. The PF activity produces both C and N increases. A delay is incorporated between PF spiking and subsequent increases in postsynaptic C and N.

(D) Time courses of the variables defining the model (C + N, C, and W) for different relative intervals between CF and PF spikes (NMDAR-based version of the model). The interval during which LTP occurs is shaded pink, while the LTD period is shaded blue.

(E) The CF arrives shortly after the PF burst. The simultaneous crossing of plasticity and LTD thresholds results in a net depression.

(D and F) A small LTP arises from a distant CF before (D) and after (F) PF input. The numbers from 1 to 9 correspond to the time points in (D)–(F) that are reported in (G).

(G) The evolution of C and N variables can be represented as a trajectory on the C-N plane (NMDAR-based version of the model). θ_D is the threshold between LTP and LTD regions. Plasticity develops depending on the time the synapse spends in the LTP or LTD regions. The LTP region is shaded pink and the LTD region is shaded blue. The pink, magenta, and green trajectories represent the simulations of (D)–(F), respectively, with dots representing maxima after each stimulation pulse. The number labels correspond to time points in (D)–(F).

(H) Net plasticity as a function of PF-CF interval (Safo and Regehr, 2008), in which a CF action potential precedes or follows a burst of seven PF action potentials. The dotted and solid lines plot the simulated plasticity with the Linear-N and the NMDAR-based version of the model, respectively. Points for the intervals shown in (D)–(F) are in the image. The black circles and error bars are the data from Safo and Regehr (2008), the red open circles and error bars are our own data.

together sufficient to induce both LTD and LTP postsynaptically at the PF-PC synapse (Lev-Ram et al., 1997, 2002; Boxall and Garthwaite, 1996; Namiki et al., 2005). To examine how different outcomes could arise from the activity of shared signaling mechanisms, we developed a parsimonious mechanistic model based upon three premises: (1) presynaptic NO production and postsynaptic Ca control both LTP and LTD; (2) the postsynaptic Ca concentration determines the sign of plasticity (Coesmans et al., 2004); and (3) there is an optimal delay between PF and CF activity in plasticity induction (Safo and Regehr, 2008). We further refined the first two rules by the observation that, when compared to LTD, LTP appears to depend on stronger NO signaling (longer PF bursts) and weaker PC Ca signals (no CF activity) (Figure 2; illustrated in Figures 6A and 6B). Synaptic efficacy changes depend then on two postsynaptic pathways. One, driven by postsynaptic Ca; the activity of the pathway is represented in our model by the variable C. The other is a NO-driven pathway whose activity is represented by the variable N (Figure 6C). These variables do not directly represent Ca and NO concentrations, but rather the activity of their downstream signaling pathways. Finally, we have developed two model variants of NO production; a simple version of the model, based on linear increases in N as a result of PF spikes (Linear-N) and a more detailed version of the model reflecting NMDAR activation in which at least two spikes in close succession are needed to trigger an increase in the N variable (NMDAR-based version) (see Supplemental Information).

Both PF and CF activity can drive the C variable (with the CF generating a larger C signal than PFs), while the N variable depends only on PF activity. At any point in time during an induction protocol, a synapse will have associated with it a pair of values (C and N). We can therefore represent the plasticity variables for

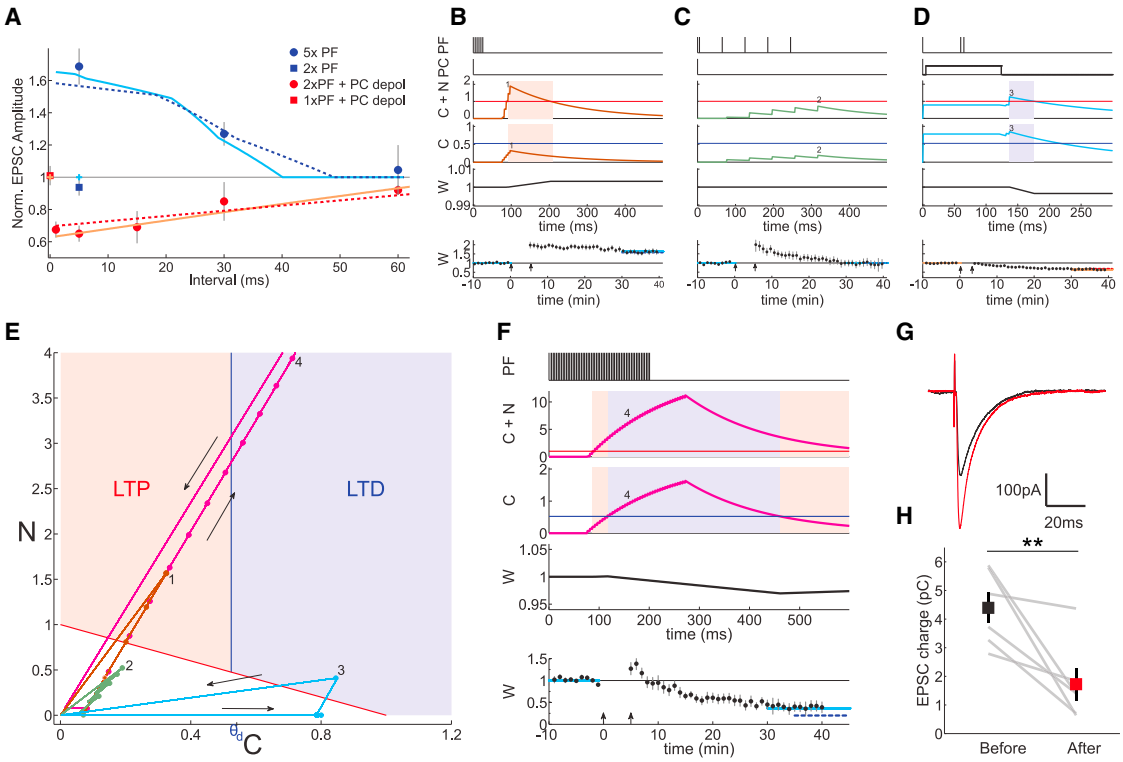

Figure 7. Relationship between PF Activity Patterns with or without PC Depolarization and PF-PC Synaptic Plasticity in the Model

(A) High pass filter plasticity rule at the PF-PC synapse. The blue circles show experimental data from Figure 2: bursts of 5× PF stimuli at different frequencies. The blue square shows experimental data from Figure 2: bursts of 2× PF stimuli at 200 Hz. The red circles show experimental data from Bidoret et al. (2009): bursts of 2× PF stimuli at different frequencies combined with PC depolarization. The red square shows experimental data from Bidoret et al. (2009): single 1× PF stimulus combined with PC depolarization. The blue line shows fitting of the model for 5× PF stimuli at different frequencies. The red line shows fitting of the model for 2× PF stimuli at different frequencies plus PC depolarization. The dashed and solid lines show the fit of the Linear-N and the NMDAR-based versions of the model, respectively. The blue and red crosses show fitting of the model for 2× PF at 200 Hz and 1× PF plus PC depolarization, respectively. Both versions of the model yielded identical fits for these two conditions.

(B) A burst of five PF action potentials at 200 Hz leads to plasticity (C + N > 1, shaded area), which is LTP (C < θ_D, shaded pink, see the increase of the synaptic weight W). The bottom image shows a comparison between the asymptotic synaptic efficacy in the NMDAR-based version of the model (300 bursts, solid blue line), the Linear-N version of the model (dashed blue line), and experimental data from Figure 2 (black dots).

(C) Similar simulation of 300 low-frequency (16.7 Hz) bursts (five pulses). This protocol leads to no plasticity.

(D) Two PF action potentials at 200 Hz coupled to PC depolarization lead to plasticity (C + N > 1, shaded area), which is LTD (C > θ_D, shaded blue, see the decrease of W). The bottom image shows a comparison between the asymptotic synaptic efficacy in the NMDAR-based version of the model (120 bursts, solid red line), the Linear-N version of the model (dashed red line), and experimental data from Bidoret et al. (2009) (black dots).

(E) Trajectories in the C-N plane for the protocols shown in (B)–(D) and (F) for the NMDAR-based version of the model. The PF activity generates diagonal trajectories that remain below the plasticity threshold (green, C), extend into the LTP region (brown, B), or when combined with CF or as part of a longer burst reach well into the LTD region (blue and magenta, D and F). The number labels correspond to time points in (B)–(D) and (F).

(F) Simulation for 300 high-frequency (200 Hz) long bursts (40 pulses). The synapse spends most of the time above the plasticity threshold in the LTD region. The model therefore predicts a net LTD. The prediction for long-term weight changes (W) after 300 repetitions is plotted. The number 4 label corresponds to the time point reported in (E). The black dots show the time course of the EPSC charge in experiments verifying the prediction that 40-pulse high-frequency bursts should induce LTD (n = 6) (bottom). The blue dashed and solid lines show the prediction from the Linear-N and the NMDAR-based versions of the model, respectively.

(G) Representative recordings from the experiments in (F). The traces are averages of 15 sweeps, before (black) and after (red) induction.

(H) Individual experiments. A summary of the EPSC charge before (black square) and after plasticity induction (red square).

one synapse as a point moving in the C-N plane. We divided the C-N plane into three regions according to the nature of the plasticity induced. The first region, containing the origin (low C and low N), induces no plasticity. The second region (LTP region), is characterized by high N and low C values (C < θ_D; θ_D being a threshold for plasticity sign). The third and final region (LTD region), is characterized by larger C value (C > θ_D) and extends to lower N values than the LTP region. Using numerical optimization techniques, we obtained the parameter set for each version of the model that best fits the model to a coherent set of 17 different experimental protocols (Safo and Regehr, 2008; Bidoret et al., 2009; this paper; see parameter sets in Table S1). These studies were chosen to have similar experimental conditions: age, temperature, and divalent ion concentrations. These experiments characterize: (1) the effects of different intervals between PF and CF stimulation in both LTP and LTD (Safo and Regehr, 2008) (Figure 6), (2) frequency and burst-length dependence of PF-induced LTP (this paper, see Figures 7A–7C and 7E), and

(3) frequency and burst-length dependence of PF with PC depolarization in inducing LTD (Bidoret et al., 2009) (Figures 7A, 7D, and 7E). Both versions of the model provide good fits to the data, with the NMDAR-based version of the model resulting in a significantly better fit, even when correcting for the additional parameter (the decay of the NMDAR activation state, see Supplemental Information).

The model could reproduce the relation between CF delay and PF weight change (Wang et al., 2000; Safo and Regehr, 2008; Figure 6). A protocol in which a CF stimulation preceded seven PF stimulations by 170 ms is shown in Figure 6D. In the C-N plane, the threshold for plasticity is the straight line C + N = 1. This threshold is also shown as a horizontal line on the C + N time course. The sign of the plasticity is then determined by whether $C > \theta_D$ or not. On the C time course, the LTP/LTD threshold θ_D (C = 0.522) is shown (Figures 6D–6F). In Figure 6G (orange line), the initial CF stimulation causes an immediate and large horizontal shift (1), which then decays toward the origin. Before it has relaxed completely, the responses from the PF stimuli cause successive upward/rightward shifts with brief relaxations toward the origin in between (2 to 4). Only toward the end of the train does the trajectory cross into the plasticity region, crossing the LTP region to visit briefly the edge of the LTD region, before returning to the origin. Because most of the time above the plasticity threshold is spent in the LTP region, a small potentiation results.

The time courses of two other protocols are shown in Figures 6E and 6F. In the first, the conjunction of CF and PF responses causes the C + N = 1 plasticity threshold to be crossed with $C > \theta_D$ for most of the time, causing LTD. This is the magenta trajectory in the C-N plane of Figure 6G. In the second, the green trajectory and time course of Figure 7C show a protocol in which the CF response arrives long after the PF responses and therefore LTP is produced. The resulting synaptic weight changes are plotted as a function of the CF-PF interval in Figure 6H and compared with the data of Safo and Regehr (2008). For experimental confirmation, we reproduced part of these data (open red dots). With a single delay parameter, our model is able to reproduce the optimal interval for depression, the magnitude of depression, the interval range over which depression is observed, and the overshooting potentiation for intervals far from the depression optimum.

Both versions of the model fit the dependency on PF frequency and burst length determined in this paper for LTP induction in Figure 2 (Figures 7A–7C and 7E), although the version incorporating the NMDAR activation better fits the data. The same set of parameter values can also account for the varying LTD amplitudes reported in a previous study (Bidoret et al., 2009; Figures 7A, 7D, and 7E). In this report, LTD was analyzed as a function of different frequencies of PF stimulation combined with PC depolarization.

A key feature of our model is that both LTP and LTD under physiological conditions require increases of Ca and NO, with the sign of the result depending upon the intensity of the Ca signal. The difference between inducing LTP and LTD thus seems to be a quantitative one, not a qualitative one. This led us to consider the possibility that PF activity alone might be able to induce LTD. Simulations using the same parameter set indicated that longer trains of PF stimuli should induce LTD rather than LTP (Figures 7E and 7F), as the synapse would spend much more time in the LTD than in the LTP region (see Supplemental Information). We tested this prediction by applying 200 Hz bursts of 40 stimuli, repeated at 1 Hz for 5 min. The result of this experiment is shown in Figures 7G and 7H. We observed a robust LTD (42 ± 11%, n = 6, p = 0.003, and $p = 1.5 \times 10^{-5}$ versus five pulses), in striking contrast with the LTP obtained with shorter bursts in Figures 2, 7A, and 7B.

In summary, a single set of model parameters representing the signaling pathways of postsynaptic Ca and presynaptic NO is able to account for the induction of LTP and LTD in a large set of experiments obtained under equivalent conditions.

DISCUSSION

Presynaptic NMDARs in Parallel Fibers Are Functional

We have previously proposed a mechanism requiring activation of presynaptic NMDARs to explain the properties of LTD induction at the cerebellar synapse between PFs and PCs (Bidoret et al., 2009). However, general acceptance of this scheme has suffered from the lack of direct evidence of Ca permeation through presynaptic NMDARs. Indeed, the existence and location of presynaptic NMDARs have been debated and alternative mechanisms have been proposed for LTD induction. In particular, the NMDAR/NOS signaling cascade has been proposed to operate in interneurons (Shin and Linden, 2005; Wang et al., 2014). In the adult, postsynaptic NMDAR activation at the CF-PC synapse has also been suggested to be necessary for LTD induction at the PF-PC synapse (Piochon et al., 2010), though PCs are devoid of functional NMDARs in young rodents (Piochon et al., 2007; Bidoret et al., 2009).

Here, we have presented direct experimental evidence for the presence of functional presynaptic NMDARs in PFs. We have imaged a large population of individual varicosities in PFs. Upon high-frequency burst stimulation, PF varicosities exhibited increases of intracellular Ca that were reversibly attenuated by bath application of D-APV. In contrast, the Ca responses to lower-frequency bursts were insensitive to D-APV. Analysis of the behavior of individual varicosities revealed what appeared to be two distinct populations. In the majority population, Ca signals were not sensitive to D-APV. However, in the second group (about 30%), D-APV significantly decreased Ca signals when the stimulation frequency was high. The frequency specificity is consistent with the requirement for HFS during plasticity induction. This ~30% D-APV sensitive subset of varicosities is in good agreement with the reported fraction of 24% PF varicosities expressing NMDAR subunits as detected by immunohistochemistry (Bidoret et al., 2009). Expression of NMDARs only in a small fraction of varicosities could also provide an explanation for the negative results obtained with bulk imaging (Shin and Linden, 2005).

It is worthwhile considering briefly the properties of the fraction of synapses that may express presynaptic NMDARs. Approximately 80% of PF-PC synapses have been estimated to be "silent" (undetectable in typical electrophysiological experiments) (Isope and Barbour, 2002), raising the possibility of

a link between the functional state of a synapse and the presence or absence of presynaptic NMDARs. In this regard, we point out that LTD depends upon NMDAR activation, implying that some non-silent synapses must be among those expressing these receptors.

NMDARs Define the Presynaptic Contribution to the PF-PC Plasticity Rule

We have described the activity patterns that produce LTP at the PF-PC synapse. LTP is induced by repetitive activity of PFs without concomitant CF activity. LTP occurs when PFs fire high-frequency bursts. We confirmed the physiological relevance of a high-frequency learning rule in vivo, where this range of PF firing frequency had been previously observed (Chadderton et al., 2004). This aspect of the learning rule is the same as described for LTD (Bidoret et al., 2009). In addition, and in contrast with LTD, LTP induction needs longer bursts (five spikes work, three do not). We propose that these two parameters of the learning rule (frequency and duration of the bursts) could be determined by the biophysical properties of NMDARs. After a release event in PFs, glutamate may bind to presynaptic NMDA autoreceptors. Since the depolarization associated with the action potential is short (less than a millisecond), by the time glutamate binds to the receptor and promotes its opening, Mg ions may block permeation. Current flow and Ca entry through NMDARs will only occur if PFs fire again before glutamate dissociates. This may set a plasticity rule that selects high-frequency repetitive firing of the presynaptic element.

We have tested the NMDAR dependence of LTP induction. LTP is fully blocked by NMDAR antagonists and is abolished in animals were NMDARs have been knocked out specifically in granule cells. Moreover, only rapidly deactivating NMDARs can account for the selection of the high-frequency firing patterns required. Only NMDARs composed of GluN1 plus GluN2A subunits have such fast deactivation. We have tested pharmacologically the subunit composition of the NMDARs involved in LTP induction. These have a clear GluN1/GluN2A pharmacological profile, as already demonstrated for LTD (Bidoret et al., 2009). We have further confirmed this molecular profile using GluN2A KO mice. The GluN2A nature of the NMDARs present in varicosities and responsible for plasticity induction is an additional argument against the involvement of receptors in molecular layer interneurons. At this age, interneurons have been shown to express essentially GluN2B and GluN2D-containing NMDARs (Bidoret et al., 2015; Dubois et al., 2016). Interestingly, GluN2A KO mice present deficits in cerebellar motor learning, but not in basal motor performance. In particular, conditioned eyeblink responses are impaired in these mice (Kishimoto et al., 1997). Furthermore, they have deficits in phase reversal adaptation of their vestibulo-ocular reflex (VOR), while their basic eye movement performance is normal (Andreescu et al., 2011). This phenotype has been proposed to depend on a functional defect at the mossy fiber to granule cell synapse, but VOR adaptation deficits have been traditionally ascribed to problems in PF-PC synaptic plasticity.

Besides depending on NMDARs, LTP induction also requires NO signaling. NO may be produced in the following way. Activation of presynaptic NMDARs allows Ca influx that activates NOS, which is often tightly coupled to the NMDARs (Christopherson et al., 1999). NO then diffuses to the postsynaptic side of the synapse. In agreement with a direct link between NMDAR activation and NO synthesis, it has recently been shown that PF burst activity produces NO in an NMDAR-dependent manner (Wang et al., 2014). NO activation of guanylate cyclase (sGC) has been shown to be necessary for LTD induction (Boxall and Garthwaite, 1996; Lev-Ram et al., 1997). In contrast, the targets of NO during LTP induction are unknown, although it is known that sGC is not required (Lev-Ram et al., 2002). The fact that LTP induction appears to require more PF action potentials (five suffice and three do not) per burst than LTD (two suffice) is also suggestive of a different postsynaptic target. If this target had a lower affinity for NO or was more distant from the point of NO synthesis, a more sustained production of NO would be necessary for LTP induction, as we observed.

The NMDAR dependence of LTP is in apparent conflict with previous reports (Wang et al., 2014; Piochon et al., 2010; Canepari and Vogt, 2008). This discrepancy can originate from the recording conditions. Among these, in the parasagittal slices used in previous studies, the stimulation electrode is close to the recorded synapses. In these conditions, unintentional electroporation of cell membranes around the stimulating electrode (Hamann and Attwell, 1996; Figure S2D) might allow Ca influx and spurious NOS activation. The NO produced in this way would reach the recorded synapses, which are close to the stimulation electrode in the sagittal orientation, bypassing the requirement for NMDAR activation. Our experiments were performed in transverse slices, where PFs can be stimulated at greater distances from the recorded synapses (100–500 μm). At this distance, normal presynaptic Ca dynamics are preserved (Figures 5B and 5C).

We note that other forms of plasticity may be present at PF-PC synapses, in particular those associated with the shifts between silent and functional states. These other forms of plasticity may use different signaling pathways, may be NMDAR independent, and their rules may depend on different types of activity patterns.

A Unified, Predictive Model Defining the PF-PC Synaptic Plasticity Rule

We were able to reproduce all the principal aspects of the experimentally determined plasticity rules using a deliberately parsimonious model based on two variables, one driven by postsynaptic Ca and the other by NO. A plasticity threshold that depends on both variables, plus an LTP-LTD Ca threshold, can explain the majority of the spike-pattern-based plasticity literature for the PF-PC synapse, at least that obtained under comparable experimental conditions. The C + N threshold enforces the high-pass filter on PF activity seen in both LTP and LTD experiments, because high-frequency activity is necessary for presynaptic NMDAR activation and/or effective summation of mediators to reach the threshold. The sign of plasticity is determined by the Ca variable (Coesmans et al., 2004).

The plasticity rule we have introduced here bears some similarities with previous Ca-based rules used to account for plasticity data in the hippocampus and neocortex (Shouval et al., 2002; Graupner and Brunel 2012). To account for PF-PC synapse data, two major modifications needed to be

introduced: potentiation occurs at lower Ca concentrations than depression in the PF-PC model, contrary to forebrain models and an additional variable, related to NO, needs to be introduced. Our model can generate predictions for plasticity outcomes for arbitrary sequences of PF and CF activity. We used the model to make and verify the prediction that bursts of PF activity could induce LTD if maintained for long enough. In addition to providing strong support for the model, this result reinforces our suggested mechanism according to which the Ca-driven signals from both PF and CF inputs are of similar nature, but different magnitude. Our model does not address the biochemical mechanisms underlying the plasticity thresholds. One can speculate about the existence of qualitative differences in Ca activation between effectors for LTP and for LTD. These differences may rely on the distance between Ca sources and targets. The different sensitivity of LTP and LTD to T-type Ca-channel block supports this possibility (Ly et al., 2013). Lacking quantitative measurement of the kinetics of NO synthesis in PFs, the simplest version of our model (Linear-N) implements identical NO generation at all action potentials including the first, yet is able to reproduce the requirement for multiple action potentials. A more detailed version of the model that implements an absence of NO production by the first action potential of a burst ("NMDAR-based" model) provides a significantly better fit of the data. A common mechanism holds in all cases, which is that effective summation of decaying responses only occurs when several arrive within an interval that is short compared to their decay time. This holds whether the integration mechanism concerns presynaptic influx of Ca through NMDARs, accumulation of mediators downstream of NO production, or both.

Non-Hebbian plasticity in cerebellar-like structures (the dorsal cochlear nucleus) has also been shown to be dependent on high-frequency activity and NMDAR activation (Fujino and Oertel, 2003), although these forms of plasticity depend on different induction mechanisms. Here, we show that presynaptic NMDARs in PFs seem to act as bursts detectors. Granule cell bursting activity may therefore be selected for plasticity induction at the PF-PC synapse and possibly for motor learning. Theoretical work (Clopath and Brunel, 2013) has shown that learning capacity at the PF-PC synapse is maximized if the variance of granule cell firing rates is maximized. So one can learn more if granule cells switch between silent and bursting, which maximizes the variance of the firing rate. Our plasticity rule would specifically operate on the bursts.

As shown by the success of the STDP rule(s), a simple, but effective, description of a plasticity rule can greatly facilitate modeling and theoretical research. We are hopeful that the relative simplicity of our model, combined with its ability to explain the relationship between complex activity patterns and plasticity outcomes, will contribute to the future deciphering of the mechanisms of learning and memory in the cerebellum.

EXPERIMENTAL PROCEDURES

Animal experimentation complied with French and European regulations. This included anesthesia and euthanasia. The "Comité d'Ethique pour l'Expérimentation Animale Charles Darwin" approved specifically in vivo experiments of the project "The cerebellar control of motor tuning during sensory discrimination" by C.L. Dossier Ce5/2012/002.

Electrophysiology in Slices

Cerebellar acute slices (300 μm) were obtained from Wistar rats and C57Bl6 mice (18- to 24-days-old). Unless otherwise stated, experiments were done in transverse slices to ensure the disruption of normal Ca dynamics that occurs close to the stimulation electrode (Figure S2D) was distant from the recorded synapses. Unless otherwise stated, cells were voltage-clamped at −70 mV in whole-cell with a K-gluconate based internal solution. Experiments were at 32°C. 20 μM bicuculline methochloride was added to block GABA-A-mediated inhibitory transmission. EPSCs were evoked by stimulating PFs extracellularly with a glass pipette at the surface of the molecular layer at 100–500 μm from the recorded PC or when indicated in the GCL at 100–200 μm. Test stimulation was applied at 0.05 Hz and consisted of two pulses separated by 100 ms, allowing PPF quantification. During induction, PCs were held in current clamp. Plasticity was quantified as the ratio between EPSC charge 30 min after induction and control EPSC charge. Further details available in Supplemental Information.

Electrophysiology In Vivo

Wistar rats were anesthetized with urethane and installed in a stereotaxic frame. PF stimulation and recording of local field potentials were done at the surface of the cerebellar vermis with tungsten microelectrodes. fEPSPs were expressed as the ratio between the slope of the synaptic response and the amplitude of the afferent volley. LTP was quantified as the ratio between fEPSP after induction and baseline.

Electroporation

Acute transgenesis through electroporation of mOrange and GCaMP5G was performed on the cerebella of P7 mice. See Supplemental Information.

Calcium Imaging

Experiments were performed with a random-access two-photon microscope. Laser was tuned to 920 nm. Fluorescence was detected after 580-30 nm filter to track PFs and 520-35 nm filter to acquire Ca signals. Individual boutons were identified as bead-like swellings along PFs. Imaging was done in the presence of NBQX (5 μM), bicuculline methochloride (20 μM), and AM-251 (1–2 μM). Experiments were at 32°C. Burst stimulations (20–25 pulses every 15 s), resulted in fluorescence peaks ranging from 1 to 50 ΔF/F. Only varicosities with low basal fluorescence, relatively large, and stable signals were retained for analysis.

Model of Synaptic Plasticity at PF-PC Synapses

We developed a mechanistic model for synaptic plasticity at the PF-PC synapse. The rationale for the model is described in the relevant section of the Results (see Figure 6C). Plasticity was considered to be controlled by two variables, which can be interpreted as intracellular signals depending on Ca and NO, respectively. See Supplemental Information.

SUPPLEMENTAL INFORMATION

Supplemental Information includes Supplemental Experimental Procedures, two figures, and one table and can be found with this article online at http://dx.doi.org/10.1016/j.celrep.2016.03.004.

AUTHOR CONTRIBUTIONS

G.B., D.H., B.B., N.B., and M.C. designed the study and experiments and wrote the manuscript. G.B. performed experiments. G.B. and M.C. analyzed and interpreted the data. D.H. contributed to their statistical analysis. D.H. and N.B. developed the model. M.S. and C.L. supported in vivo recordings. D.C. initiated electroporation. B.M. and S.D. set up the two-photon microscope.

ACKNOWLEDGMENTS

This work was supported by the program "Investissements d'Avenir" from the French Government, implemented by Agence Nationale de la Recherche

(ANR), references: ANR-10-LABX-54 MEMOLIFE and ANR-11-IDEX-0001-02 PSL* Research University. B.B. was funded by ANR-08-SYSC-005, ANR-08-BLAN-0023, and PEPS CNRS-PSL. D.H. was supported by a EU grant (CEREBNET FP7-ITN238686). N.B. was funded by ANR-08-SYSC-005 and NSF (IIS-1430296). G.B. was funded by Région Ile de France, FRM, and Labex MEMOLIFE. We thank FRC AOE-6 Rotary 2010 and France Bio imaging for funding. The funders had no role in study design, data collection and analysis, decision to publish, or preparation of the manuscript. We thank A. Ayon for help with molecular biology and P. Ascher, C. Bimbard, A. Blot, D. Debanne, A. Marty, J.C. Poncer, R. Proville, B. Stell, and L. Venance for comments on the manuscript.

Received: May 19, 2015
Revised: January 15, 2016
Accepted: February 25, 2016
Published: March 24, 2016

REFERENCES

Andreescu, C.E., Prestori, F., Brandalise, F., D'Errico, A., De Jeu, M.T., Rossi, P., Botta, L., Kohr, G., Perin, P., D'Angelo, E., and De Zeeuw, C.I. (2011). NR2A subunit of the N-methyl D-aspartate receptors are required for potentiation at the mossy fiber to granule cell synapse and vestibulo-cerebellar motor learning. Neuroscience *176*, 274–283.

Belmeguenai, A., and Hansel, C. (2005). A role for protein phosphatases 1, 2A, and 2B in cerebellar long-term potentiation. J. Neurosci. *25*, 10768–10772.

Bender, V.A., Bender, K.J., Brasier, D.J., and Feldman, D.E. (2006). Two coincidence detectors for spike timing-dependent plasticity in somatosensory cortex. J. Neurosci. *26*, 4166–4177.

Bidoret, C., Ayon, A., Barbour, B., and Casado, M. (2009). Presynaptic NR2A-containing NMDA receptors implement a high-pass filter synaptic plasticity rule. Proc. Natl. Acad. Sci. USA *106*, 14126–14131.

Bidoret, C., Bouvier, G., Ayon, A., Szapiro, G., and Casado, M. (2015). Properties and molecular identity of NMDA receptors at synaptic and non-synaptic inputs in cerebellar molecular layer interneurons. Front. Synaptic Neurosci. *7*, 1.

Boxall, A.R., and Garthwaite, J. (1996). Long-term depression in rat cerebellum requires both NO synthase and NO-sensitive guanylyl cyclase. Eur. J. Neurosci. *8*, 2209–2212.

Bredt, D.S., Hwang, P.M., and Snyder, S.H. (1990). Localization of nitric oxide synthase indicating a neural role for nitric oxide. Nature *347*, 768–770.

Canepari, M., and Vogt, K.E. (2008). Dendritic spike saturation of endogenous calcium buffer and induction of postsynaptic cerebellar LTP. PLoS ONE *3*, e4011.

Casado, M., Isope, P., and Ascher, P. (2002). Involvement of presynaptic N-methyl-D-aspartate receptors in cerebellar long-term depression. Neuron *33*, 123–130.

Chadderton, P., Margrie, T.W., and Häusser, M. (2004). Integration of quanta in cerebellar granule cells during sensory processing. Nature *428*, 856–860.

Christopherson, K.S., Hillier, B.J., Lim, W.A., and Bredt, D.S. (1999). PSD-95 assembles a ternary complex with the N-methyl-D-aspartic acid receptor and a bivalent neuronal NO synthase PDZ domain. J. Biol. Chem. *274*, 27467–27473.

Clopath, C., and Brunel, N. (2013). Optimal properties of analog perceptrons with excitatory weights. PLoS Comput. Biol. *9*, e1002919.

Coesmans, M., Weber, J.T., De Zeeuw, C.I., and Hansel, C. (2004). Bidirectional parallel fiber plasticity in the cerebellum under climbing fiber control. Neuron *44*, 691–700.

Debanne, D., Gähwiler, B.H., and Thompson, S.M. (1994). Asynchronous pre- and postsynaptic activity induces associative long-term depression in area CA1 of the rat hippocampus in vitro. Proc. Natl. Acad. Sci. USA *91*, 1148–1152.

Dubois, C.J., Lachamp, P.M., Sun, L., Mishina, M., and Liu, S.J. (2016). Presynaptic GluN2D receptors detect glutamate spillover and regulate cerebellar GABA release. J. Neurophysiol. *115*, 271–285.

Fino, E., Paille, V., Cui, Y., Morera-Herreras, T., Deniau, J.M., and Venance, L. (2010). Distinct coincidence detectors govern the corticostriatal spike timing-dependent plasticity. J. Physiol. *588*, 3045–3062.

Froemke, R.C., and Dan, Y. (2002). Spike-timing-dependent synaptic modification induced by natural spike trains. Nature *416*, 433–438.

Fujino, K., and Oertel, D. (2003). Bidirectional synaptic plasticity in the cerebellum-like mammalian dorsal cochlear nucleus. Proc. Natl. Acad. Sci. USA *100*, 265–270.

Gerstner, W., Kempter, R., van Hemmen, J.L., and Wagner, H. (1996). A neuronal learning rule for sub-millisecond temporal coding. Nature *383*, 76–81.

Goto, J., Inoue, T., Kuruma, A., and Mikoshiba, K. (2006). Short-term potentiation at the parallel fiber-Purkinje cell synapse. Neurosci. Res. *55*, 28–33.

Graupner, M., and Brunel, N. (2012). Calcium-based plasticity model explains sensitivity of synaptic changes to spike pattern, rate, and dendritic location. Proc. Natl. Acad. Sci. U S A *109*, 3991–3996.

Hamann, M., and Attwell, D. (1996). Non-synaptic release of ATP by electrical stimulation in slices of rat hippocampus, cerebellum and habenula. Eur. J. Neurosci. *8*, 1510–1515.

Isope, P., and Barbour, B. (2002). Properties of unitary granule cell–>Purkinje cell synapses in adult rat cerebellar slices. J. Neurosci. *22*, 9668–9678.

Jörntell, H., and Hansel, C. (2006). Synaptic memories upside down: bidirectional plasticity at cerebellar parallel fiber-Purkinje cell synapses. Neuron *52*, 227–238.

Kishimoto, Y., Kawahara, S., Kirino, Y., Kadotani, H., Nakamura, Y., Ikeda, M., and Yoshioka, T. (1997). Conditioned eyeblink response is impaired in mutant mice lacking NMDA receptor subunit NR2A. Neuroreport *8*, 3717–3721.

Lev-Ram, V., Jiang, T., Wood, J., Lawrence, D.S., and Tsien, R.Y. (1997). Synergies and coincidence requirements between NO, cGMP, and Ca^{2+} in the induction of cerebellar long-term depression. Neuron *18*, 1025–1038.

Lev-Ram, V., Wong, S.T., Storm, D.R., and Tsien, R.Y. (2002). A new form of cerebellar long-term potentiation is postsynaptic and depends on nitric oxide but not cAMP. Proc. Natl. Acad. Sci. USA *99*, 8389–8393.

Ly, R., Bouvier, G., Schonewille, M., Arabo, A., Rondi-Reig, L., Léna, C., Casado, M., De Zeeuw, C.I., and Feltz, A. (2013). T-type channel blockade impairs long-term potentiation at the parallel fiber-Purkinje cell synapse and cerebellar learning. Proc. Natl. Acad. Sci. USA *110*, 20302–20307.

Manabe, T., Wyllie, D.J., Perkel, D.J., and Nicoll, R.A. (1993). Modulation of synaptic transmission and long-term potentiation: effects on paired pulse facilitation and EPSC variance in the CA1 region of the hippocampus. J. Neurophysiol. *70*, 1451–1459.

Marcaggi, P., and Attwell, D. (2007). Short- and long-term depression of rat cerebellar parallel fibre synaptic transmission mediated by synaptic crosstalk. J. Physiol. *578*, 545–550.

Namiki, S., Kakizawa, S., Hirose, K., and Iino, M. (2005). NO signalling decodes frequency of neuronal activity and generates synapse-specific plasticity in mouse cerebellum. J. Physiol. *566*, 849–863.

Nowak, L., Bregestovski, P., Ascher, P., Herbet, A., and Prochiantz, A. (1984). Magnesium gates glutamate-activated channels in mouse central neurones. Nature *307*, 462–465.

Paoletti, P., Ascher, P., and Neyton, J. (1997). High-affinity zinc inhibition of NMDA NR1-NR2A receptors. J. Neurosci. *17*, 5711–5725.

Piochon, C., Irinopoulou, T., Brusciano, D., Bailly, Y., Mariani, J., and Levenes, C. (2007). NMDA receptor contribution to the climbing fiber response in the adult mouse Purkinje cell. J. Neurosci. *27*, 10797–10809.

Piochon, C., Levenes, C., Ohtsuki, G., and Hansel, C. (2010). Purkinje cell NMDA receptors assume a key role in synaptic gain control in the mature cerebellum. J. Neurosci. *30*, 15330–15335.

Rodríguez-Moreno, A., and Paulsen, O. (2008). Spike timing-dependent long-term depression requires presynaptic NMDA receptors. Nat. Neurosci. *11*, 744–745.

Safo, P., and Regehr, W.G. (2008). Timing dependence of the induction of cerebellar LTD. Neuropharmacology *54*, 213–218.

Shin, J.H., and Linden, D.J. (2005). An NMDA receptor/nitric oxide cascade is involved in cerebellar LTD but is not localized to the parallel fiber terminal. J. Neurophysiol. *94*, 4281–4289.

Shouval, H.Z., Bear, M.F., and Cooper, L.N. (2002). A unified model of NMDA receptor-dependent bidirectional synaptic plasticity. Proc. Natl. Acad. Sci. U S A *99*, 10831–10836.

Sjöström, P.J., Turrigiano, G.G., and Nelson, S.B. (2001). Rate, timing, and cooperativity jointly determine cortical synaptic plasticity. Neuron *32*, 1149–1164.

Sjöström, P.J., Turrigiano, G.G., and Nelson, S.B. (2003). Neocortical LTD via coincident activation of presynaptic NMDA and cannabinoid receptors. Neuron *39*, 641–654.

Squire, L.R., and Kandel, E.R. (2009). Memory: From Mind to Molecules, Second Edition (Roberts & Co).

Wang, S.S., Denk, W., and Häusser, M. (2000). Coincidence detection in single dendritic spines mediated by calcium release. Nat. Neurosci. *3*, 1266–1273.

Wang, X., Chen, G., Gao, W., and Ebner, T. (2009). Long-term potentiation of the responses to parallel fiber stimulation in mouse cerebellar cortex in vivo. Neuroscience *162*, 713–722.

Wang, D.J., Su, L.D., Wang, Y.N., Yang, D., Sun, C.L., Zhou, L., Wang, X.X., and Shen, Y. (2014). Long-term potentiation at cerebellar parallel fiber-Purkinje cell synapses requires presynaptic and postsynaptic signaling cascades. J. Neurosci. *34*, 2355–2364.